Brief Communications

Maturation of Na_V and K_V Channel Topographies in the Auditory Nerve Spike Initiator before and after Developmental Onset of Hearing Function

Kyunghee X. Kim and Mark A. Rutherford
Department of Otolaryngology, Washington University School of Medicine, St. Louis, Missouri 63110

Auditory nerve excitation and thus hearing depend on spike-generating ion channels and their placement along the axons of auditory nerve fibers (ANFs). The developmental expression patterns and native axonal locations of voltage-gated ion channels in ANFs are unknown. Therefore, we examined the development of heminodes and nodes of Ranvier in the peripheral axons of type I ANFs in the rat cochlea with immunohistochemistry and confocal microscopy. Nodal structures presumably supporting presensory spiking formed between postnatal days 5 (P5) and P7, including Ankyrin-G, $Na_V1.6$, and Caspr. These immature nodal structures lacked low-voltage-activated $K_V1.1$ which was not enriched at juxtaparanodes until approximately P13, concurrent with the developmental onset of acoustic hearing function. Anatomical alignment of ANF spike-initiating heminodes relative to excitatory input from inner hair cell (IHC) ribbon synapses continued until approximately P30. High-voltage-activated $K_V3.1b$ and $K_V2.2$ were expressed in mutually exclusive domains: $K_V3.1b$ was strictly localized to nodes and heminodes, whereas $K_V2.2$ expression began at the juxtaparanodes and continued centrally along the first internode. At spike-initiating heminodes in the distal osseous spiral lamina, $Na_V1.1$ partly overlapped $Na_V1.6$ and ankyrin-G. ANFs displayed $K_V7.2$ and $K_V7.3$ at heminodes, nodes, internodes, and the unmyelinated synaptic terminal segments beneath IHCs in the organ of Corti. In response to sound, spikes are initiated at the heminode, which is tightly coupled to the IHC ribbon synapse ~20–40 μm away. These results show that maturation of nodal alignment and ion channel content may underlie postnatal improvements of ANF excitability and discharge synchrony.

Key words: action potential generation; ankyrin-G; axon initial segment; cochlea; heminode; voltage-gated Na^+ and K^+ channels

Significance Statement

Acoustic and electrical hearing depends on rapid, reliable, and precise spike generation in auditory nerve fibers. A limitation of current models and therapies is a lack of information on the identities and topographies of underlying ion channels. We report the developmental profile of the auditory nerve spike generator with a focus on $Na_V1.1$, $Na_V1.6$, $K_V1.1$, $K_V2.2$, $K_V3.1b$, $K_V7.2$, and $K_V7.3$ in relation to the scaffold ankyrin-G. Molecular anatomy of the spike generator matures in the weeks after developmental onset of hearing function. Subcellular positioning of voltage-gated ion channels will enable multicompartmental modeling of auditory nerve responses elicited by afferent chemical neurotransmission from hair cells and modulated by efferent neurotransmitters or evoked by extracellular field stimulation from a cochlear implant.

Introduction

Auditory nerve fibers (ANFs) respond to sound by firing patterns of spikes, triggered by sensory inner hair cells (IHCs) at afferent ribbon synapses. Although synaptic transmission and extracellular current pulses from prosthetic electrodes stimulate ANFs very differently, the ensuing action potential relies on voltage-gated ion channels and their topographies.

Channels have been identified in ANFs (Oak and Yi, 2014; Davis and Crozier, 2015), but their native topographies remain largely unknown. Each ANF in cats and mice has a postsynaptic heminode located 20–40 μm from its presynaptic ribbon-type active zone on

Received Sept. 14, 2015; revised Nov. 25, 2015; accepted Dec. 30, 2015.

Author contributions: K.X.K. and M.A.R. designed research; K.X.K. and M.A.R. performed research; K.X.K. and M.A.R. analyzed data; K.X.K. and M.A.R. wrote the paper.

This work was funded by the Department of Otolaryngology at Washington University, an International Project Grant from Action on Hearing Loss, and the McDonnell Center for Cellular and Molecular Neurobiology Small Grants Program (M.A.R.). We thank Santa Cruz Biotechnology for generous provision of primary antibodies, K. Griffin for technical support, and M. Warchol for comments.

The authors declare no competing financial interests.

Correspondence should be addressed to Mark A. Rutherford, Department of Otolaryngology, Box 8115, Washington University in St. Louis School of Medicine, 660 S. Euclid Ave., St. Louis, MO 63110. E-mail: RutherfordM@ent.wustl.edu.

DOI:10.1523/JNEUROSCI.3437-15.2016

 0270-6474/16/362111-08$15.00/0

an IHC (Liberman, 1980; Hossain et al., 2005). Computational modeling of patch-clamp recordings from rat ANFs suggested that spikes are initiated at this heminode (Rutherford et al., 2012); however, the molecular–anatomical details of the ANF spike initiator are unclear. Here, we analyzed the development of voltage-gated Na^+ (Na_V) and K^+ (K_V) channel protein expression.

Spike initiation generally occurs where channels associate in structures called axon initial segments (AISs) positioned between dendrite and axon before the myelin begins, where firing behavior can be controlled (Bender and Trussell, 2012). The scaffold protein ankyrin-G localizes to AISs and nodes of Ranvier, where it coordinates assembly of the spectrin cytoskeleton, Na_V, and cell adhesion molecules (Kordeli et al., 1995). Common vertebrate ankyrin-G-binding motifs target $Na_V1.6$, $K_V7.2$, and $K_V7.3$ to AISs (Pan et al., 2006). Therefore, we focused on ankyrin-G-associated channels at the heminode adjacent to the habenula perforata (HP) in the distal osseous spiral lamina (OSL) of the cochlea, where EPSPs from the organ of Corti impinge on the initial axonal segments of the auditory nerve.

An increase in hearing sensitivity follows the postnatal onset of auditory function in rats. ANF activity can first be evoked through bone conduction at postnatal day 7 (P7) to P8 or through air conduction at P11–P13; ANF excitability and discharge synchrony then increase until peaking at approximately P30 (Uziel et al., 1981; Geal-Dor et al., 1993). Maturation beyond hearing onset may involve middle and inner ear mechanics, more potent transmission between IHCs and ANFs, more efficient and precise spike generation in ANFs, and refinement of efferent innervation. During maturation of ANF sound-response physiology in the first postnatal month, we find increasing ion channel colocalization on heminodes and tighter spatial alignment of heminodes relative to ribbon synapses. These changes may increase ANF excitability and reduce temporal jitter, thereby lowering auditory nerve response threshold and increasing discharge synchrony.

Materials and Methods

Immunohistochemistry. Wistar rats of either sex were used as approved by the Animal Studies Committee of Washington University. Whole-mounts and cryosections were prepared as described previously (Jing et al., 2013; Kim et al., 2014). Primary antibodies: $Na_V1.1$ (mouse; NeuroMab), $Na_V1.6$ (goat; Santa Cruz Biotechnology), Pan-Na_V1 (mouse; NeuroMab), $K_V1.1$ (rabbit; Santa Cruz Biotechnology), $K_V2.2$ (rabbit; Alomone Laboratories), $K_V3.1b$ (rabbit; Alomone Laboratories), $K_V7.2$ (goat; Santa Cruz Biotechnology), $K_V7.3$ (rabbit; Santa Cruz Biotechnology), Caspr (mouse; NeuroMab), ankyrin-G (mouse, NeuroMab; goat or rabbit, Santa Cruz Biotechnology), Na^+/K^+-ATPase $\alpha3$ (mouse, Life Technologies; goat, Santa Cruz Biotechnology), Calretinin (mouse; Santa Cruz Biotechnology), and MyosinVIIa (rabbit; Proteus Biosciences) were used with Alexa Fluor 488-, 555-, and 647-conjugated secondary antibodies.

Confocal microscopy and image analysis. Volumes were sampled with z-step of 0.38 μm and pixel size of 100 nm on a Zeiss LSM700. Maximum-intensity projections were made with ImageJ. Fluorescence intensity profiles and particle positions were analyzed with IGOR Pro (Wavemetrics). Colocalization was measured with Volocity (PerkinElmer) using Manders' colocalization coefficients (M_1 and M_2) with automatic thresholding (Costes et al., 2004; Dunn et al., 2011). M_1 is the ratio of the summed intensities of pixels where both protein-1 and protein-2 are located relative to the summed intensities of all pixels with protein-1. Average M values of 0.99 were measured at heminodes when a primary antibody was simultaneously reacted with two secondary antibodies emitting on different wavelengths.

Results

We studied postnatal development in cochlear primary afferent neurons, also called type I spiral ganglion neurons, herein referred to as ANFs. We first recognized ankyrin-G immunoreactivity as filamentous structures in the OSL at P5. By P6 in the basal cochlea and P7 in the apical cochlea (Fig. 1*A*,*B*), we observed alignment of these filamentous structures near the small holes in the bony shelf of the OSL, the HP. The region central to the HP, in the distal-most OSL, is the region on each mature ANF where the heminode lies and the myelin sheath begins (schematized in Fig. 2*H*). As development proceeded through the second and third postnatal weeks, ankyrin-G became restricted to a domain immediately adjacent to the HP (Fig. 1*C*,*D*). Peripheral to the HP, the terminal of each ANF receives synaptic input in the neuropil under IHCs called the inner spiral plexus (ISP), where we did not detect ankyrin-G immunoreactivity on ANFs.

Ankyrin-G colocalization with Na_V during myelination of auditory neurons

To examine the formation of heminodes and nodes of Ranvier in the distal OSL, we applied antibodies for the intracellular scaffold protein ankyrin-G, the voltage-gated sodium channel α subunit $Na_V1.6$, and the contactin-associated protein Caspr. Marking paranodes, the edges of contact between Schwann cell myelin and ANF axons, Caspr was apparent by P8 in the apical cochlea (Fig. 1*A*) and by P6 in the base (Fig. 1*B*), consistent with the onset of myelination (Romand and Romand, 1985).

We detected $Na_V1.6$ adjacent to Caspr by P9, ~2 d after the appearance of ankyrin-G in the OSL of the apical cochlea. The basal cochlea developed similarly, preceding the apex by ~2 d. The appearance of these immature nodes (arrowheads in Fig. 1*A*,*B*) coincided with the developmental emergence of ANF electrical activity in response to bone-conducted vibrations (Geal-Dor et al., 1993), which bypass outer and middle ear immaturities. In the following days and weeks, ankyrin-G, $Na_V1.6$, Pan-Na_V1 (recognizing all α subunits), and $K_V3.1b$ became restricted to a region within a few micrometers central to the HP (Fig. 1*C*–*E*).

Approximately 4 d after the onset of acoustic hearing, ankyrin-G appeared nearer to the HP than $Na_V1.6$ and still covered a larger area than did $Na_V1.6$ at heminodes (Fig. 1*E*, top, P17). $Na_V1.6$ and ankyrin-G overlapped more completely at nodes (Fig. 1*E*, middle and bottom). To compare heminodes and nodes in the distal OSL, we performed colocalization analysis throughout postnatal development. The colocalization statistics M_1 and M_2, ranging from 0 to 1, quantify the degree of spatial overlap between two signals. M_2 is the ratio of the summed intensities of pixels where both protein-1 and protein-2 are located relative to the summed intensities of all pixels with protein-2. At heminodes near the HP, the M_2 values all increased from P11 to P30 (Fig. 1*F*, bottom left). In contrast, M_2 values for nodes were already maximal by P11 (Fig. 1*F*, bottom right). This is consistent with a distinct requirement for ankyrin-G in clustering of Na_V at spike-initiating heminodes compared with spike-propagating nodes, as demonstrated in rat dorsal root ganglion neurons (Dzhashiashvili et al., 2007).

At heminodes, M_2 of $Na_V1.6$ with ankyrin-G (($Na_V1.6 \cap$ Ank-G)/Ank-G) was always smaller than M_2 of Pan-Na_V1 with ankyrin-G (Fig. 1*F*, bottom left), suggesting the presence of another Na_V1 subunit in the ankyrin-G domain. $Na_V1.1$ and $Na_V1.7$ were reported in cochlear spiral ganglion (Fryatt et al., 2009) and $Na_V1.2$ in cochlear efferents (Hossain et al., 2005). $Na_V1.6$ was located on ANF heminodes and nodes. However, we found $Na_V1.1$ immunoreactivity at heminodes only (Fig. 1*G*, P20), potentially accounting for the incomplete overlap of $Na_V1.6$ with ankyrin-G at heminodes compared with nodes.

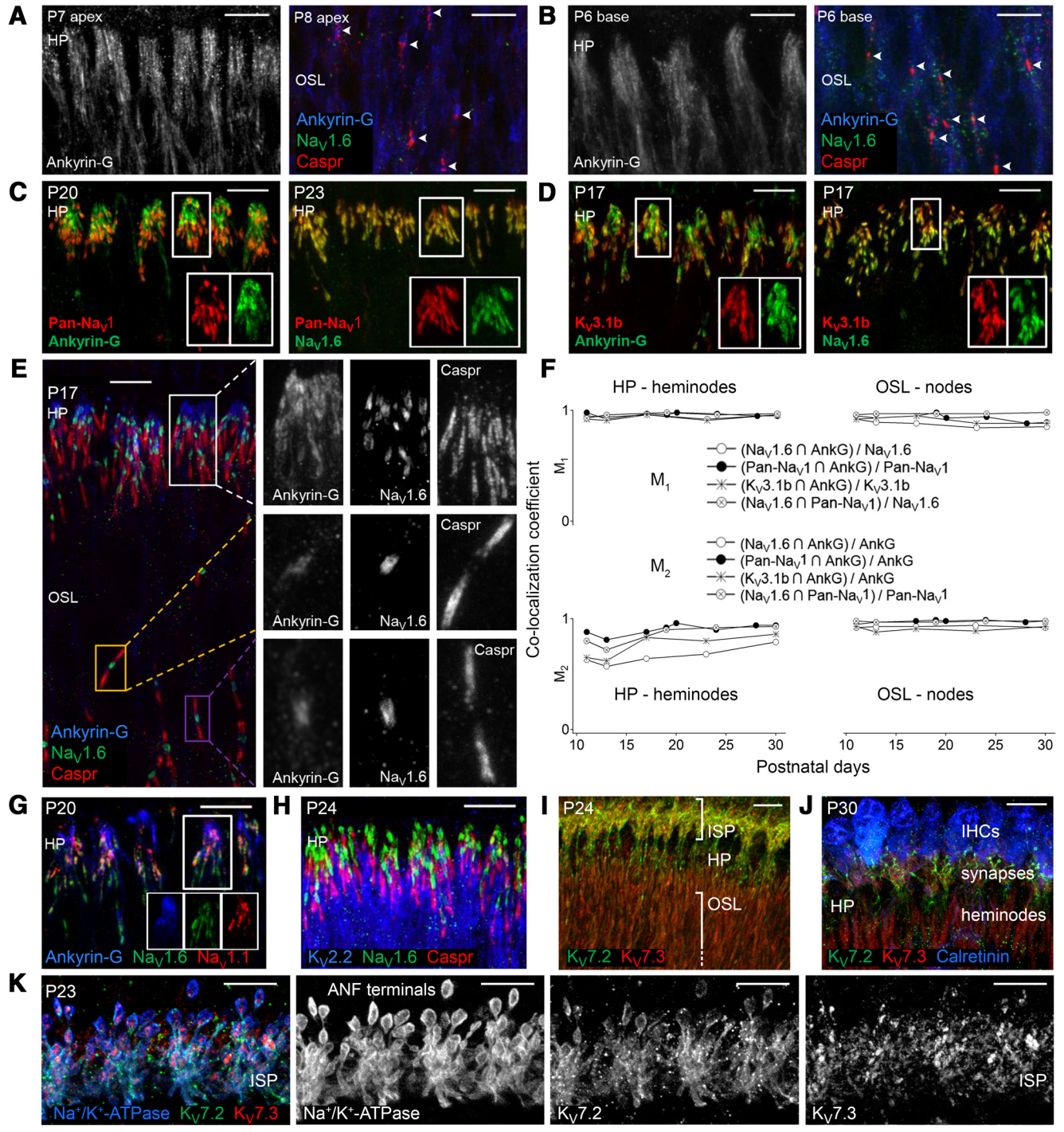

Figure 1. Ion channel localization with ankyrin-G. ***A***, ***B***, Ankyrin-G aligned at the HP in the apical cochlea by P7 and in the basal turn by P6 as nodes developed (arrowheads). ***C***, Pan-Na_V1 colocalized with ankyrin-G and $Na_V1.6$ near the HP. ***D***, $K_V3.1b$ colocalized with ankyrin-G and $Na_V1.6$. ***E***, View of HP and distal OSL with enlargements in grayscale for heminodes at the HP (top row) and nodes in the OSL (bottom rows). ***F***, M_1 and M_2 (top and bottom, respectively, see Materials and Methods) versus postnatal day for heminodes (left) and nodes (right) illustrate the development of colocalization. ROIs ($n = 20–210$ per data point) were determined by outlining regions near the HP ($\sim 70\ \mu m^2$) or OSL ($\sim 4\ \mu m^2$). SEM ranged from 0.00 to 0.03 (data not shown). Spatial overlap with ankyrin-G increased over development for Pan-Na_V1, $Na_V1.6$, and $K_V3.1b$; $M_{2,P30} > M_{2,P11}$, $p < 10^{-4}$, Student's two-tailed t test. ***G***, At heminodes, $Na_V1.1$ partially overlapped $Na_V1.6$ and ankyrin-G. ***H***, $K_V2.2$ expression extended from juxtaparanodes centrally. ***I–K***, $K_V7.2$ and $K_V7.3$ expression in the OSL, at the HP, and in the ISP under IHCs. ***J***, Calretinin-labeled IHCs. ***K***, Na^+/K^+-ATPase-labeled ANF membranes. Scale bars, 10 μm.

Distinct membrane topographies of K_V channels in ANFs

Like Na_V1 with ankyrin-G, we also found a developmental increase in colocalization of the delayed rectifier $K_V3.1b$ with ankyrin-G. Indeed, the largest change in M_2 was the increase in colocalization of $K_V3.1b$ with ankyrin-G between P13 and P17, immediately after hearing onset (Fig. 1*F*, bottom left). In stark contrast to the confinement of $K_V3.1b$ to heminodes (Fig. 1*D*) and nodes (data not shown), the slower delayed rectifier $K_V2.2$ was present throughout fibers in the OSL but was excluded from heminodes and paranodes specifically where Na_V and Caspr resided, respectively (Fig. 1*H*).

We next probed for K_V7 in ANFs (Jin et al., 2009), known in other cell types for influencing excitability and binding directly to ankyrin-G (Schwarz et al., 2006; Rasmussen et al., 2007). $K_V7.2$ and $K_V7.3$ were detected throughout ANF axons in the OSL (Fig. 1*I*, P24)

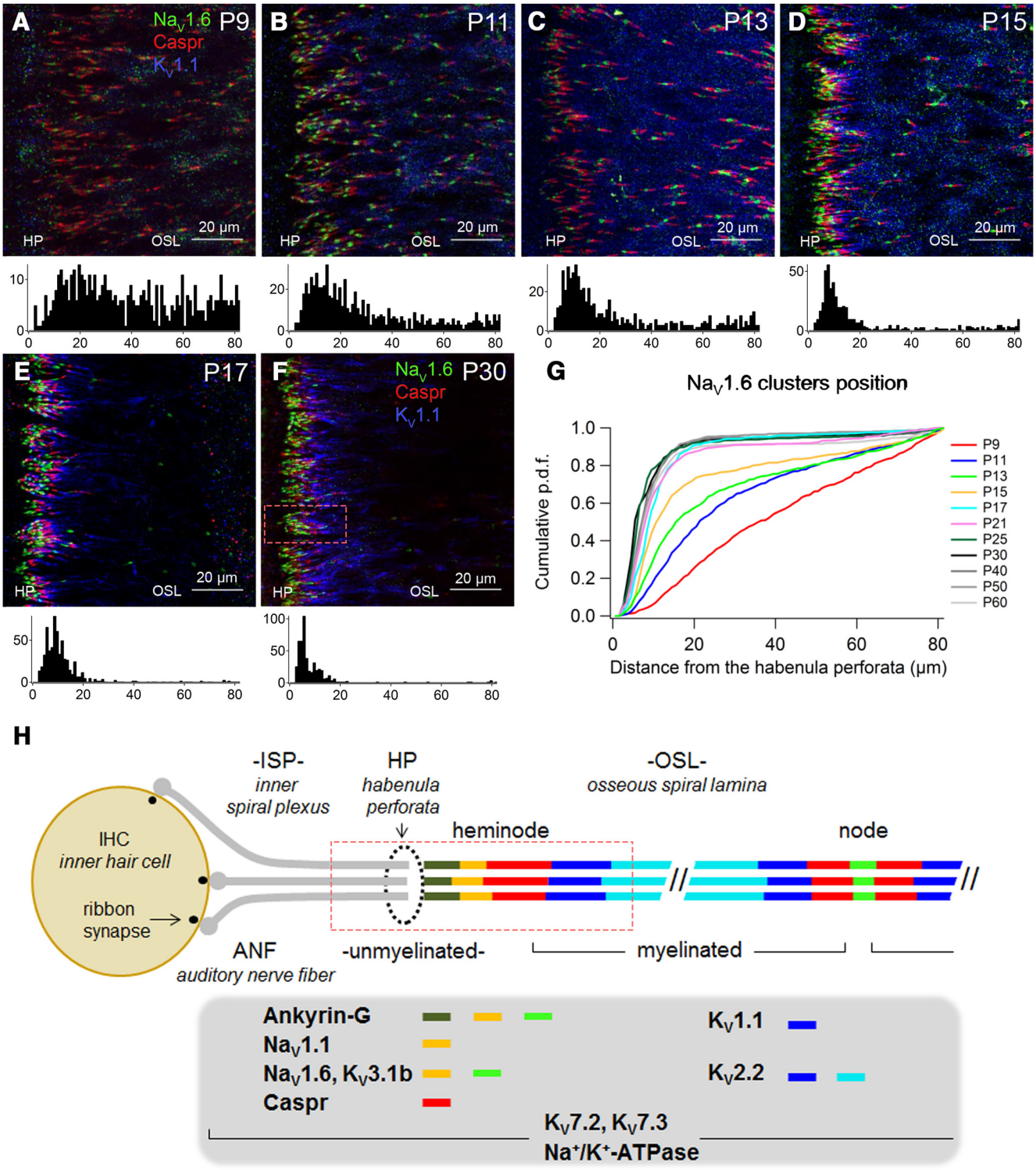

Figure 2. Developmental alignment of heminodes, $Na_V1.6$. ***A–F***, ANFs in the distal OSL from P9 –P60. Bottom, Frequency histograms of $Na_V1.6$ cluster position (in micrometers from HP; $n = 3$ images each). ***G***, Normalized cumulative probability density functions for the postnatal days indicated (≥3 whole-mounts from ≥2 animals each). Alignment changed most rapidly from P9 to P17. Comparison of P9 with P11, of P11 with P15, or of P15 with P17 revealed significant differences (Kolmogorov–Smirnov test, $p \leq 0.02$). The fraction of clusters centered within 20 μm of the HP reached a maximum of 92% at P30. ***H***, Schematic of IHC with three ANFs showing placement of ion channels at mature heminodes and nodes.

and they each overlapped with ankyrin-G on fibers near the HP (data not shown). In addition, and in contrast to the other Na_V and K_V channels probed here, $K_V7.2$ and $K_V7.3$ were detected in the neuropil under IHCs in the ISP, partially overlapping the neuronal membrane marker Na^+/K^+-ATPase (Fig. 1*J*,*K*).

Spike generator maturation beyond the onset of hearing function

To observe the formation of (hemi)nodes, paranodes, and juxtaparanodes, we probed for $Na_V1.6$, Caspr, and $K_V1.1$, respectively (Mi et al., 1995; Arroyo et al., 1999). Figure 2 measures the positions of $Na_V1.6$ clusters. At P9, immature nodes of Ranvier

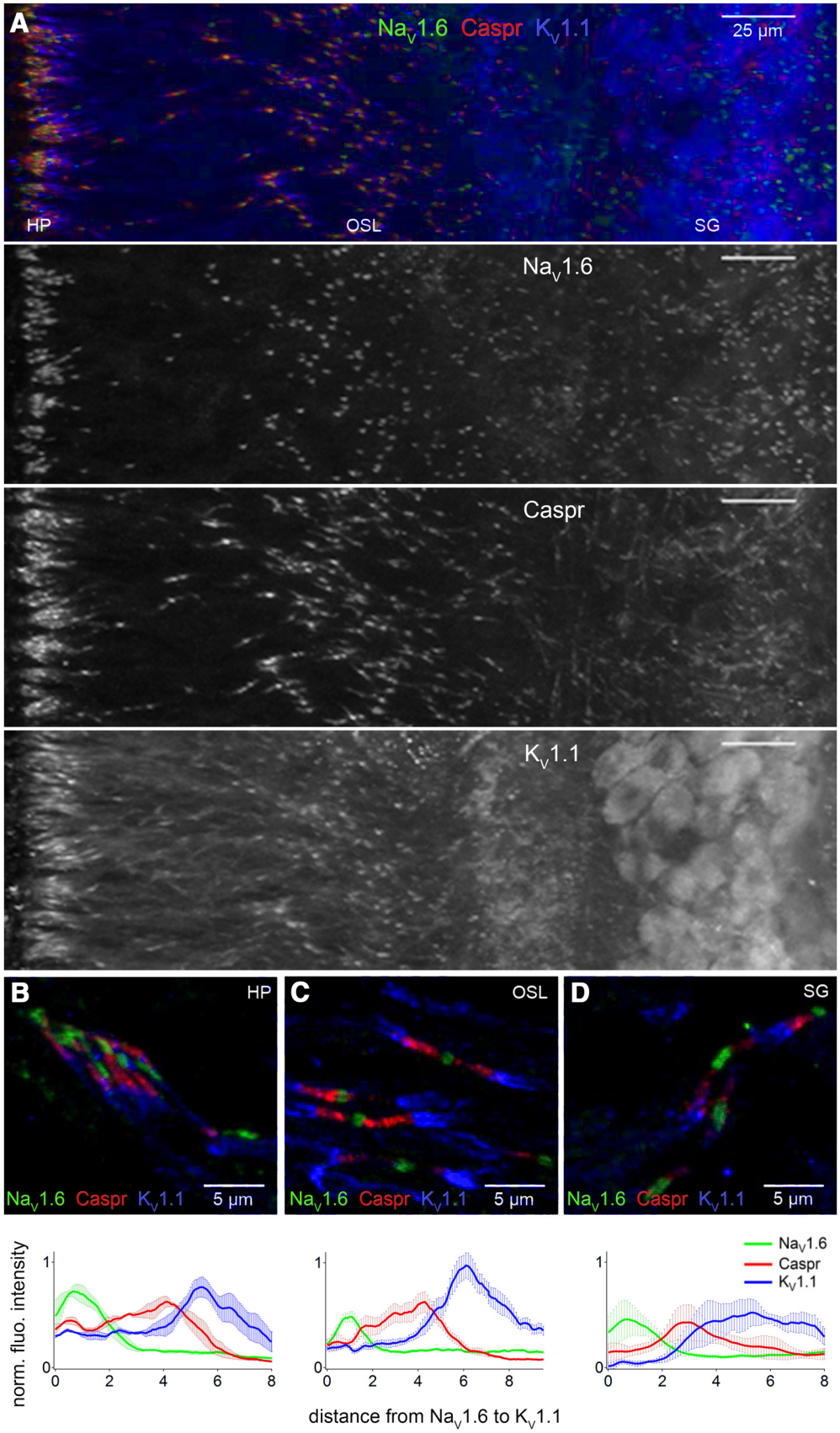

Figure 3. Similar structure of heminodes and nodes in ANF peripheral axons. ***A***, $Na_V1.6$, Caspr, and $K_V1.1$ from heminodes by the HP to somas in the spiral ganglion (SG; P21, whole-mount). ***B–D***, Cryosections showing heminodes and nodes by the HP (***B***, P23), in the OSL (***C***, P25), and in the SG (***D***, P23). Line plots show mean (±SEM) fluorescence intensity as a function of distance along the structure from $Na_V1.6$ to $K_V1.1$ ($n = 3$, 10, and 4 in ***B–D***, respectively). Structures were aligned at the center of $Na_V1.6$.

appeared in the OSL as $Na_V1.6$ clusters, flanked on both sides by Caspr but apparently lacking $K_V1.1$ (Fig. 2*A*). By P15, all three proteins clustered near the HP in heminode formation (Fig. 2*B–D*). The largest developmental changes in heminode alignment were complete by P17 in the apical cochlear turn, when most $Na_V1.6$ clusters were centered within 10 μm of the HP. We detected smaller, slower improvements of heminode alignment up to P25–P30 (Fig. 2*F*, *G*). Between P15 and P30, $K_V1.1$ expression concentrated at juxtaparanodes (Fig. 2*D–F*) as internodes lengthened beyond 80 μm from the HP (Figs. 3, 4). Results for the mature ANF are summarized in Figure 2*H*.

Molecular microdomain structure is similar within heminodes and nodes

Spikes initiated at the heminodes are propagated at nodes on ANF peripheral axons (Figs. 3, 4) and then across somas and along central axons to the brain. Line profiles suggested that $Na_V1.6$, Caspr, and $K_V1.1$ distributions were similar, on average, within structures in three locations: near the HP, in the middle of the OSL, and in the spiral ganglion. Heminode or half-node length, defined here as center of $Na_V1.6$ cluster to center of $K_V1.1$ cluster (node to juxtaparanode), with Caspr between them, was ~5 μm on average (Fig. 3*B–D*).

Discussion

Maturation of the spike generator after hearing onset

We observed initial formation of nodal structures with immunohistochemistry between P6 and P9 (Figs. 1, 2). These immature nodes presumably conduct patterned presensory spontaneous activity from the organ of Corti to the brain (Geal-Dor et al., 1993; Tritsch and Bergles, 2010). Heminode alignment and channel colocalization with ankyrin-G progressed until approximately P30 (Figs. 1*F*, 2). These changes may underlie the decreased latency and increased synchrony of ANF discharge in the weeks after hearing onset (Uziel et al., 1981).

In contrast to nodes, heminodes exhibited a sustained increase in colocalization of ankyrin-G with $Na_V1.6$ and $K_V3.1b$ over postnatal development to P30 (Fig. 1*E*,*F*). Heminode alignment paralleled maturation of myelination: the number of myelin lamellae around ANF peripheral axons increased until P30 (Romand and Romand, 1985). Together, these results suggest that ANF heminode alignment depends on lengthening of the internode plus confinement of Na_V1 channels to the ankyrin-G domain.

In mature ANFs, $K_V1.1$ was present throughout axons and somas but enriched at juxtaparanodes, $K_V2.2$ was expressed uniformly along internodes, $K_V3.1b$ was located strictly at heminodes and nodes, and $K_V7.2$ and $K_V7.3$ were detected in myelinated and unmyelinated segments in the OSL and ISP (Figs. 1, 2, 3). $Na_V1.6$ colocalized with $K_V3.1b$ at heminodes and nodes, whereas $Na_V1.1$ located to heminodes only (Fig. 1). Future work should determine how the distinct topographies of these ion

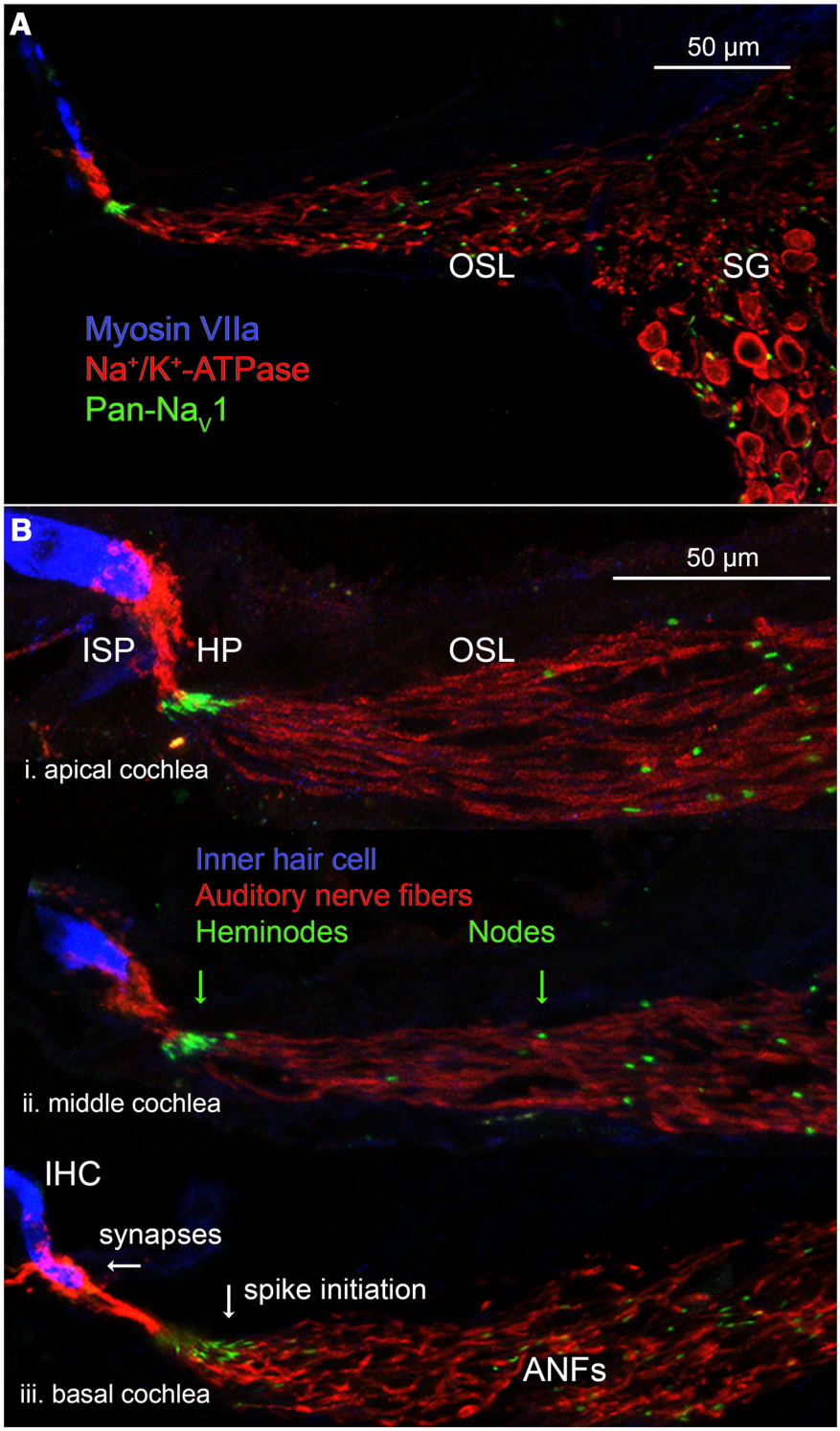

Figure 4. Overview of Na_V1 channels on ANFs in radial sections. ***A***, Mid-modiolar cryosections provide a view orthogonal to the whole-mount (Fig. 3). ANFs are labeled with Na^+/K^+-ATPase from synaptic terminals with IHCs on the left (MyosinVIIa) to the spiral ganglion on the right. ***B***, Immunolabeling for PanNa_V1 in the apical, middle, and basal cochlear turns (P22). Short, thin unmyelinated segments in the ISP connect synapses with heminodes. Longer, thicker internodes connect heminodes to nodes in the OSL.

channels complement their unique electrophysiological properties to shape the auditory nerve's representation of sound.

$Na_V1.1$ and $Na_V1.6$ are expressed with ankyrin-G at the ANF spike initiator

On the distal-most segment of mature ANFs, we found Na_V1 channels restricted to a short cluster positioned immediately central to the HP in whole-mounts and cryosections (Figs. 1, 2, 3, 4). This is consistent with another confocal whole-mount study in rat (McLean et al., 2009), but different from an epifluorescence cryosection study in mice concluding that $Na_V1.6$ was also present on the unmyelinated terminals of ANFs in the organ of Corti (Hossain et al., 2005).

In addition to $Na_V1.6$, we found $Na_V1.1$ overlapping with ankyrin-G at heminodes (Fig. 1*G*). $Na_V1.1$ currents may be inhibited through activation of G-protein-coupled neurotransmitter receptors (Cantrell and Catterall, 2001). Dopamine receptors are expressed on ANF heminodes postsynaptic to lateral olivocochlear efferents (Maison et al., 2012) positioned to modulate spike initiation and thus auditory sensitivity. Future work should determine whether $Na_V1.6$ and $Na_V1.1$ are distributed heterogeneously within or among ANF heminodes, as they are at the AISs of different functional types of motoneurons (Duflocq et al., 2011).

Heminode length was ~5 μm (Figs. 3, 4). The ANF postsynaptic heminode is significantly shorter in length than presynaptic or postsynaptic heminodes at the next two stages of auditory signal processing: at the endbulb of Held synapses between ANFs and globular bushy cells in the anteroventral cochlear nucleus (Spirou et al., 2005) and at the calyx of Held synapses between globular bushy cells and medial nucleus of the trapezoid body (MNTB) neurons, where $Na_V1.6$ seems to be the major isoform (Leão et al., 2005).

K_V channels of distinct class and topography in ANFs

The placement of K_V channels with different voltage-dependent properties in distinct locations along axons may be a crucial determinant of ANF firing properties. The high-voltage-activated potassium channels are triggered by depolarization to mediate repolarization of the membrane potential. We found $K_V3.1b$ confined to heminodes and nodes. Whereas K_V3 channels turn on and off with the rising and falling phases of the action potential, the slower K_V2 channels may hyperpolarize the interspike potential and thereby expedite recovery of Na_V channels from inactivation. Such a mechanism was suggested for MNTB neurons, in which $K_V2.2$ channels were enriched on one part of the AIS (Johnston et al., 2008). The role of $K_V2.2$ channels awaits investigation in ANFs, in which they are positioned along internodes (Fig. 1*H*).

Low-voltage-activated potassium channels may support phasic response properties by producing spike thresholds that depend on depolarization rate, as they do in some auditory brain neurons (Svirskis et al., 2002). $K_V1.1$ and $K_V1.2$ are expressed in ANFs and recordings from dissociated ganglion cells show that these channels subserve rapid adaptation at stimulus onset (Mo et al., 2002; Lacas-Gervais et al., 2004; Smith et al., 2015). We found that $K_V1.1$ was enriched at juxtaparanodes beginning after the onset of hearing (Fig. 2). The absence of $K_V1.1$ in distal axons before P10 may be important for allowing presensory spiking in ANFs, which is crucial for the development of the auditory brainstem (Clause et al., 2014) because synaptic excitation from immature IHCs is relatively slow (Grant et al., 2010).

The voltage-gated M-currents generally have slower kinetics, are partly activated at the resting potential, and are carried mainly by $K_V7.2$ and $K_V7.3$. In contrast to the other K_V channels studied here, we found $K_V7.2$ and $K_V7.3$ within the organ of Corti under IHCs (Fig. 1*I–K*). The relative abundance of K_V7 subunits appeared to change along ANFs, with $K_V7.2$ being greater in the ISP than the OSL and $K_V7.3$ being greater in the OSL than the ISP. K_V7 channels were also found in the calyx terminals of vestibular primary afferent neurons under utricular hair cells (Lysakowski et al., 2011). M-channels may be modulated by synaptic activity to influence neuronal firing properties through G-protein-coupled receptors (Brown and Passmore, 2009). Therefore, like the hyperpolarization-activated cyclic nucleotide-gated channels and K_V1 channels (Yi et al., 2010; Liu et al., 2014; Negm and Bruce, 2014), our results show that K_V7 and K_V2 channels may be crucial determinants of acoustic and electrical signal representation in ANFs.

Auditory nerve AIS is tightly coupled to synaptic input

ANFs are bipolar, having myelinated axons in two directions from their ganglionic somas: one distally ~300 μm to the organ of Corti (Figs. 3, 4) and one centrally ~1 mm to the brain. If the short 20–40 μm unmyelinated postsynaptic terminal segment in the organ of Corti is the dendrite, then the heminode separates the dendrite from the distal myelinated axon. If the electrical length constant of type I ANFs is much longer than 20–40 μm, as it is for type II ANFs (Weisz et al., 2012), then the type I ANF postsynaptic terminal and its spike-initiating AIS would be nearly isopotential. We conclude that the ANF heminode displays molecular–anatomical specializations of an AIS and suggest that it is the preferred site of action potential initiation.

References

Arroyo EJ, Xu YT, Zhou L, Messing A, Peles E, Chiu SY, Scherer SS (1999) Myelinating Schwann cells determine the internodal localization of Kv1.1, Kv1.2, Kvbeta2, and Caspr. J Neurocytol 28:333–347. CrossRef Medline

Bender KJ, Trussell LO (2012) The physiology of the axon initial segment. Annu Rev Neurosci 35:249–265. CrossRef Medline

Brown DA, Passmore GM (2009) Neural KCNQ (Kv7) channels. Br J Pharmacol 156:1185–1195. CrossRef Medline

Cantrell AR, Catterall WA (2001) Neuromodulation of Na+ channels: An unexpected form of cellular plasticity. Nat Rev Neurosci 2:397–407. Medline

Clause A, Kim G, Sonntag M, Weisz CJ, Vetter DE, Rűbsamen R, Kandler K (2014) The precise temporal pattern of prehearing spontaneous activity is necessary for tonotopic map refinement. Neuron 82:822–835. CrossRef Medline

Costes SV, Daelemans D, Cho EH, Dobbin Z, Pavlakis G, Lockett S (2004) Automatic and quantitative measurement of protein-protein colocalization in live cells. Biophys J 86:3993–4003. CrossRef Medline

Davis RL, Crozier RA (2015) Dynamic firing properties of type I spiral ganglion neurons. Cell Tissue Res 361:115–127. CrossRef Medline

Duflocq A, Chareyre F, Giovannini M, Couraud F, Davenne M (2011) Characterization of the axon initial segment (AIS) of motor neurons and identification of a para-AIS and a juxtapara-AIS, organized by protein 4.1B. BMC Biol 9:66. CrossRef Medline

Dunn KW, Kamocka MM, McDonald JH (2011) A practical guide to evaluating colocalization in biological microscopy. Am J Physiol Cell Physiol 300:C723–C742. CrossRef Medline

Dzhashiashvili Y, Zhang Y, Galinska J, Lam I, Grumet M, Salzer JL (2007) Nodes of Ranvier and axon initial segments are ankyrin G-dependent domains that assemble by distinct mechanisms. J Cell Biol 177:857–870. CrossRef Medline

Fryatt AG, Vial C, Mulheran M, Gunthorpe MJ, Grubb BD (2009) Voltage-gated sodium channel expression in rat spiral ganglion neurons. Mol Cell Neurosci 42:399–407. CrossRef Medline

Geal-Dor M, Freeman S, Li G, Sohmer H (1993) Development of hearing in

neonatal rats: air and bone conducted ABR thresholds. Hear Res 69: 236–242. CrossRef Medline

Grant L, Yi E, Glowatzki E (2010) Two modes of release shape the postsynaptic response at the inner hair cell ribbon synapse. J Neurosci 30:4210–4220. CrossRef Medline

Hossain WA, Antic SD, Yang Y, Rasband MN, Morest DK (2005) Where is the spike generator of the cochlear nerve? Voltage-gated sodium channels in the mouse cochlea. J Neurosci 25:6857–6868. CrossRef Medline

Jin Z, Liang GH, Cooper EC, Jarlebark L (2009) Expression and localization of K channels KCNQ2 and KCNQ3 in the mammalian cochlea. Audiol Neurootol 14:98–105. CrossRef Medline

Jing Z, Rutherford MA, Takago H, Frank T, Fejtova A, Khimich D, Moser T, Strenzke N (2013) Disruption of the presynaptic cytomatrix protein bassoon degrades ribbon anchorage, multiquantal release, and sound encoding at the hair cell afferent synapse. J Neurosci 33:4456–4467. CrossRef Medline

Johnston J, Griffin SJ, Baker C, Skrzypiec A, Chernova T, Forsythe ID (2008) Initial segment Kv2.2 channels mediate a slow delayed rectifier and maintain high frequency action potential firing in medial nucleus of the trapezoid body neurons. J Physiol 586:3493–3509. CrossRef Medline

Kim KX, Sanneman JD, Kim HM, Harbidge DG, Xu J, Soleimani M, Wangemann P, Marcus DC (2014) Slc26a7 chloride channel activity and localization in mouse Reissner's membrane epithelium. PLoS One 9:e97191. CrossRef Medline

Kordeli E, Lambert S, Bennett V (1995) AnkyrinG. A new ankyrin gene with neural-specific isoforms localized at the axonal initial segment and node of Ranvier. J Biol Chem 270:2352–2359. CrossRef Medline

Lacas-Gervais S, Guo J, Strenzke N, Scarfone E, Kolpe M, Jahkel M, De Camilli P, Moser T, Rasband MN, Solimena M (2004) BetaIVSigma1 spectrin stabilizes the nodes of Ranvier and axon initial segments. J Cell Biol 166:983–990. CrossRef Medline

Leão RM, Kushmerick C, Pinaud R, Renden R, Li GL, Taschenberger H, Spirou G, Levinson SR, von Gersdorff H (2005) Presynaptic Na^+ channels: locus, development, and recovery from inactivation at a high-fidelity synapse. J Neurosci 25:3724–3738. CrossRef Medline

Liberman MC (1980) Morphological differences among radial afferent fibers in the cat cochlea: an electron-microscopic study of serial sections. Hear Res 3:45–63. CrossRef Medline

Liu Q, Manis PB, Davis RL (2014) I_h and HCN channels in murine spiral ganglion neurons: tonotopic variation, local heterogeneity, and kinetic model. J Assoc Res Otolaryngol 15:585–599. CrossRef Medline

Lysakowski A, Gaboyard-Niay S, Calin-Jageman I, Chatlani S, Price SD, Eatock RA (2011) Molecular microdomains in a sensory terminal, the vestibular calyx ending. J Neurosci 31:10101–10114. CrossRef Medline

Maison SF, Liu XP, Eatock RA, Sibley DR, Grandy DK, Liberman MC (2012) Dopaminergic signaling in the cochlea: receptor expression patterns and deletion phenotypes. J Neurosci 32:344–355. CrossRef Medline

McLean WJ, Smith KA, Glowatzki E, Pyott SJ (2009) Distribution of the Na, K-ATPase alpha subunit in the rat spiral ganglion and organ of corti. J Assoc Res Otolaryngol 10:37–49. CrossRef Medline

Mi H, Deerinck TJ, Ellisman MH, Schwarz TL (1995) Differential distribution of closely related potassium channels in rat Schwann cells. J Neurosci 15:3761–3774. Medline

Mo ZL, Adamson CL, Davis RL (2002) Dendrotoxin-sensitive K+ currents contribute to accommodation in murine spiral ganglion neurons. J Physiol 542:763–778. CrossRef Medline

Negm MH, Bruce IC (2014) The effects of HCN and KLT ion channels on adaptation and refractoriness in a stochastic auditory nerve model. IEEE Trans Biomed Eng 61:2749–2759. CrossRef Medline

Oak MH, Yi E (2014) Voltage-gated K(+) channels contributing to temporal precision at the inner hair cell-auditory afferent nerve fiber synapses in the mammalian cochlea. Arch Pharm Res 37:821–833. CrossRef Medline

Pan Z, Kao T, Horvath Z, Lemos J, Sul JY, Cranstoun SD, Bennett V, Scherer SS, Cooper EC (2006) A common ankyrin-G-based mechanism retains KCNQ and NaV channels at electrically active domains of the axon. J Neurosci 26:2599–2613. CrossRef Medline

Rasmussen HB, Frøkjaer-Jensen C, Jensen CS, Jensen HS, Jørgensen NK, Misonou H, Trimmer JS, Olesen SP, Schmitt N (2007) Requirement of subunit co-assembly and ankyrin-G for M-channel localization at the axon initial segment. J Cell Sci 120:953–963. CrossRef Medline

Romand R, Romand MR (1985) Qualitative and quantitative observations of spiral ganglion development in the rat. Hear Res 18:111–120. CrossRef Medline

Rutherford MA, Chapochnikov NM, Moser T (2012) Spike encoding of neurotransmitter release timing by spiral ganglion neurons of the cochlea. J Neurosci 32:4773–4789. CrossRef Medline

Schwarz JR, Glassmeier G, Cooper EC, Kao TC, Nodera H, Tabuena D, Kaji R, Bostock H (2006) KCNQ channels mediate IKs, a slow K+ current regulating excitability in the rat node of Ranvier. J Physiol 573:17–34. CrossRef Medline

Smith KE, Browne L, Selwood DL, McAlpine D, Jagger DJ (2015) Phosphoinositide modulation of heteromeric Kv1 channels adjusts output of spiral ganglion neurons from hearing mice. J Neurosci 35:11221–11232. CrossRef Medline

Spirou GA, Rager J, Manis PB (2005) Convergence of auditory-nerve fiber projections onto globular bushy cells. Neuroscience 136:843–863. CrossRef Medline

Svirskis G, Kotak V, Sanes DH, Rinzel J (2002) Enhancement of signal-to-noise ratio and phase locking for small inputs by a low-threshold outward current in auditory neurons. J Neurosci 22:11019–11025. Medline

Tritsch NX, Bergles DE (2010) Developmental regulation of spontaneous activity in the mammalian cochlea. J Neurosci 30:1539–1550. CrossRef Medline

Uziel A, Romand R, Marot M (1981) Development of cochlear potentials in rats. Audiology 20:89–100. CrossRef Medline

Weisz CJ, Lehar M, Hiel H, Glowatzki E, Fuchs PA (2012) Synaptic transfer from outer hair cells to type II afferent fibers in the rat cochlea. J Neurosci 32:9528–9536. CrossRef Medline

Yi E, Roux I, Glowatzki E (2010) Dendritic HCN channels shape excitatory postsynaptic potentials at the inner hair cell afferent synapse in the mammalian cochlea. J Neurophysiol 103:2532–2543. CrossRef Medline